JOURNAL OF Materials Feature Article CHEMISTRY

Relevant examples of intercalation–deintercalation processes in solid state chemistry: application to oxides†

J-C. Grenier,*[a] J-M. Bassat,[a] J-P. Doumerc,[a] J. Etourneau,[a] Z. Fang,[b] L. Fournes,[a] S. Petit,[a] M. Pouchard[a] and A. Wattiaux[a]

[a]*Institut de la Chimie de la Matière Condensée de Bordeaux, C.N.R.S., Av. du Dr. A. Schweitzer, 33 608 Pessac Cedex, France. E-mail: grenier@chimsol.icmcb.u-bordeaux.fr.*
[b]*Institute of Physics, the Chinese Academy of Sciences, P.O. Box 603, 100080 Beijing, China*

Received 4th May 1998, Accepted 6th July 1998

Four '*chimie douce*' synthetic methods, to which much attention has been devoted in the last years, are described. The electrochemical potential is shown to be efficient for intercalating as well as for deintercalating oxygen atoms in oxides. Gaseous NO_2 is able to destroy *in situ* ammonium ions either in a soft way or violently, leading to the formation of tunneled or lamellar structures or to oxide nanoparticles. Borohydride solutions appear very attractive for the synthesis of low valent oxides at room temperature. Typical examples of these methods are given and the most important features of these reactions are discussed.

Introduction

Until the 1960s, most solid state compounds were prepared using high temperature treatments of starting materials that were first ground and pressed. Then new preparative methods were investigated at mild temperatures with the aim of synthesizing new compounds, generally unstable at high temperatures: that was the beginning of the '*chimie douce*' era. These methods can be classified in different ways according to the following features: all of them involve 'precursors' that must be tailored with respect to the desired final material; the reaction temperature ranges between room temperature and nearly 300 °C, a lower temperature leading usually to poorer crystallization; from a structural viewpoint, they can be either topotactic or reconstructive; and finally, such reactions may or not imply redox processes.

Nowadays, the largest scale technical applications of this 'soft solid state chemistry' are undoubtedly concerned with batteries. The reactions are typically intercalation–deintercalation of either cationic (Li^+, H^+) or neutral species (Li or H_2) at room temperature; the former involve redox processes and hence mixed valence oxides [*e.g.* $MnO_{2-x}(OH)_x$, Li_xNiO_2, *etc.*], the latter deal with alloys such as $LaNi_5$, metals (Al) or graphite.[1]

This paper reports on some methods recently developed for preparing oxides by either chemical or electrochemical oxidation or reduction of an appropriate precursor. The common feature of these methods is their efficiency even at room temperature. Descriptions and relevant examples of the following four methods are given: (a) electrochemical oxidation resulting in oxygen intercalation into oxide networks; (b) deintercalation of oxygen using electrochemical reduction; (c) chemical oxidation using NO_2 gas; and (d) chemical reduction using borohydride solutions.

†Basis of the presentation given at Materials Chemistry Discussion No. 1, 24–26 September 1998, ICMCB, University of Bordeaux, France.

(a) Electrochemical oxidation

In 1990, we discovered that using the electrochemical potential as a 'driving force', it was possible to intercalate oxygen into oxide networks, at room temperature, and correspondingly to overoxidize oxides up to unexpected oxygen stoichiometries.[2] Basically this reaction can be achieved thanks to the high oxygen activity resulting from an applied overpotential η on an oxide ceramic electrode according to the reaction:

$$4OH^- \rightarrow O_{2(g)}\uparrow + 2\ H_2O + 4e^-$$

$$(E_{th}{}^0 = 0.303\ \text{V}\ \textit{vs.}\ \text{Hg/HgO, at pH} = 14) \qquad (1)$$

Using the Nernst equation, one can estimate this oxygen activity to be equivalent, at room temperature for a few hundred mV of overpotential, to a very high oxygen pressure. Indeed, such activity can induce the formation of oxide films on metal electrodes. This has been recently used for growing tailored thick films of oxides such as Al_2O_3, ZnO, CuO, *etc.*,[3] but they are usually passivating. However, by replacing a metallic electrode by an oxide and provided that a diffusion path exists within the oxide matrix, oxygen atoms have been shown to migrate easily.

The most striking result was obtained in 1990 for La_2CuO_4: this insulating antiferromagnetic compound was transformed within a few hours into a metallic and superconducting oxide with $T_C = 44$ K, the highest transition temperature ever obtained for this phase.[4]

Experimental

The electrochemical system used for these experiments consists of a power supply (a potentiostat) and an electrochemical cell of three-electrode type, using alkaline solution, 1 M NaOH or KOH, as electrolyte. The electrolyte concentration of 1 M (pH = 14) is considered as the optimal one. Fig. 1 shows a scheme of the electrochemical cell, the major components of which are the three electrodes.

The working electrodes are usually ceramic pellets of the materials to be oxidized: their relative densities are around 80%, which seems to be the optimal density allowing good permeation of the electrolyte into the ceramic. A rotating working electrode is preferred to a fixed one as it produces better convection between the electrolyte in the ceramic electrode and in the bulk solution. It also prevents evolved gas bubbles (O_2), if any, from accumulating on the electrode surface. A stable and ohmic contact between the ceramic pellet and the metallic support (made of brass) which is connected with the external circuit, is required for the electrochemical process and meaningful data measurements. The assembly is achieved thanks to a gold foil and silver paste, the whole being embedded in a resin.

The reference electrode is a mercury–mercury oxide electrode

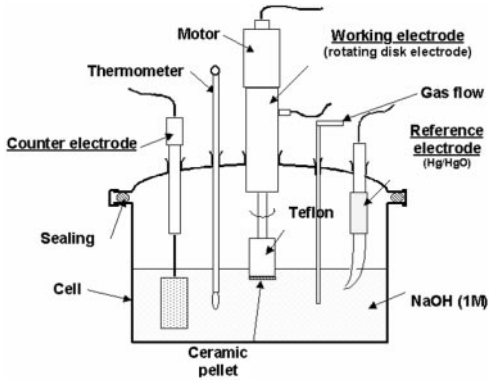

Fig. 1 The electrochemical cell with three electrodes for experiments at 25 °C–90 °C.

(Hg/HgO) that has excellent stability in alkaline solutions. Its standard potential (at $a_{OH^-}=1$ and $T=298$ K) is 0.098 V relative to SHE. All the potentials quoted in this work are referred to this electrode.

The counter electrode is designed to have a large surface area. The materials usually used are good electronic conductors, such as gold or platinum foil, or a piece of glassy carbon.

Electrochemical aspects

Various compounds $A_xM_zO_y$ whose structures derive from perovskite, have been oxidized: they belong essentially to the so-called $A_nM_nO_{3n-1}$ and $A_{n+1}M_nO_{3n+1}$ series with A = La, Nd, Sr or Ba and M = Fe, Co, Ni and Cu. The oxidation reaction can be summarized as follows:

$$A_xM_yO_z + 2\delta\ OH^- \rightarrow A_xM_yO_{z+\delta} + \delta H_2O + 2\delta e^- \qquad (2)$$

δ representing the amount of inserted oxygen. The fact that oxygen atoms and not hydroxide OH^- species are intercalated, was earlier demonstrated by several groups using various techniques such as TGA and chemical analysis, coulometric titration, ^{1}H NMR, IR and Mössbauer spectroscopies (see examples below).

Fig. 2 shows a typical *I–E* voltammetry curve (anodic part) measured on a rotating electrode. This example is concerned with the brownmillerite-type $Sr_2Co_2O_5$ material. Three regions can be seen in this curve: a linear part immediately after the polarization begins (C_1, $E<300$ mV) assigned to the charging of the double layer on the interface between the electrolyte and the electrode surface.[5] Then a wave-shaped part (O_1, $E=$ 300–450 mV) with the half-wave potential about $E_{1/2}=$ 330 mV: this is ascribed to the oxidation of the electrode material according to reaction (2). In this case it corresponds formally to the transformation from Co^{3+} to Co^{4+}. At higher potentials the current intensity increases again and the evolution of gaseous oxygen takes place in the third region (O_2, $E>450$ mV) according to reaction (1).

Then two kinds of experiments can be performed. (i) Potentiostatic oxidation, using a steady potential set in the oxidation plateau, depending on the starting material (*e.g.* 400 mV for $Sr_2Co_2O_5$). The oxidation reaction is followed by measuring the time dependence of the rest potential: the open circuit voltage, E_{OCV}, measured after 15 min, increases with the polarization time. Actually it can be directly correlated to the chemical composition, *i.e.* to the oxygen stoichiometry $(3-y)$ or to the amount of $Co^{2+}/Co^{3+}/Co^{4+}$ (Fig. 3). It shows a logarithmic dependence on the oxygen composition, which may be explained in a similar way as for the intercalation of lithium ions into CoO_2, MnO_2 or other oxides on the basis of the Armand equation.[6] The end of the polarization reaction is reflected in a drastic increase of the rest potential. (ii) Galvanostatic experiments, which are more convenient for controlling the reaction kinetics, have been used by several groups. As for the lithium intercalation into dichalcogenides or oxides, using small current intensities (a few μA), potential steps are observed. Such a feature characterizes the formation of single phases. Examples are given in Fig. 4. Thus the existence of two phases is definitively evidenced in the $La_2CuO_{4+\delta}$ system ($\delta\approx0.04$ and 0.09); they exhibit superconducting transitions at 32 and 44 K, respectively. Similarly, in the $SrCoO_{3-y}$ system, several steps are observed involving again the formation of various intermediate phases before the last stage of oxidation that leads to the fully oxidized material $SrCoO_3$. Similar features have also been reported for $La_2NiO_{4+\delta}$ and $Nd_2NiO_{4+\delta}$, which confirms the close analogy with cationic intercalation phenomena.

Table 1 summarizes the most significant results obtained during the last few years.[7–17]

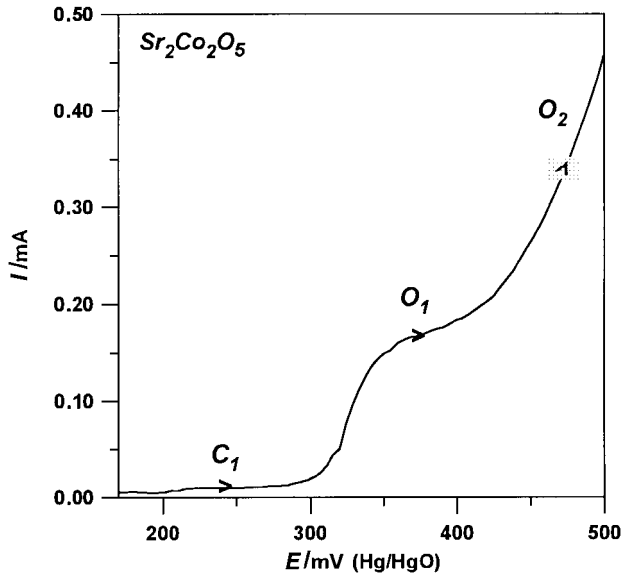

Fig. 2 Voltammetry curve (anodic part) of a brownmillerite $Sr_2Co_2O_5$-type electrode in a 1 M NaOH solution (RDE 2000 rpm, $dE/dt=$ 150 mV min^{-1}, $T=300$ K, under air). Note the oxidation plateau O_1 observed before the oxygen evolution.

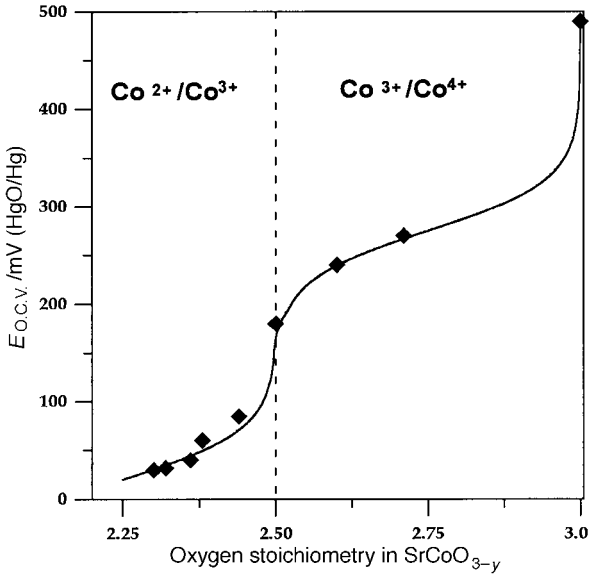

Fig. 3 Dependence of the rest potential (E_{OCV} is recorded after 15 min) on the oxygen composition of $SrCoO_{3-y}$. It shows two branches agreeing with the Armand equation $E_{OCV}=f(\delta)\propto\log\ [\delta/(1-\delta)]$, δ being the amount of inserted species.

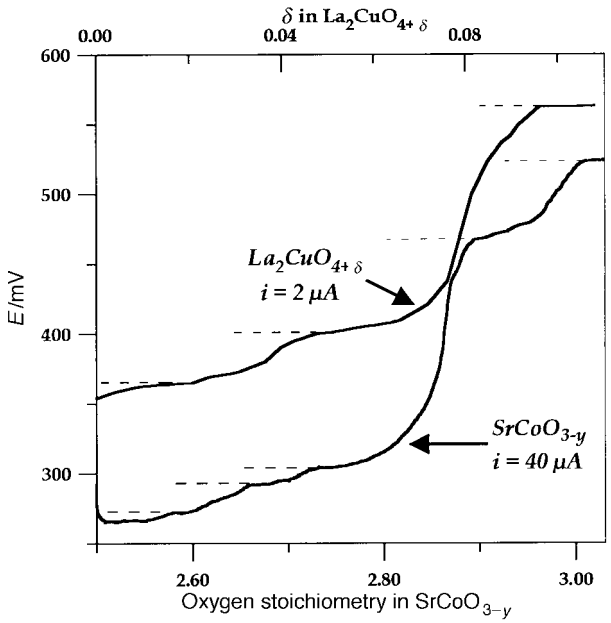

Fig. 4 Variation of the O.C.V. potential *vs.* the oxygen composition (δ) for $La_2CuO_{4+\delta}$ and $(3-y)$ for $SrCoO_{3-y}$ calculated from the overall charge transfer and reaction (2) for galvanostatic experiments.

Structural aspects

The main structural types that have been studied are represented in Fig. 5, all of them being related to the perovskite structure.

The $A_nM_nO_{3n-1}$ series. These compounds can be considered as oxygen deficient perovskites AMO_{3-y} ($n \geqslant 2$; $0 \leqslant y \leqslant 0.5$); their structures obviously exhibit channels perpendicular to the z axis, which can constitute diffusion paths for intercalating oxygen atoms. However, this precondition is not sufficient as some compounds, especially those containing calcium, do not intercalate oxygen. A tentative and simple model can be proposed by calculating the electrostatic potentials along the channels, which was performed for $Ca_2Fe_2O_5$, $Sr_2Fe_2O_5$ and $Sr_2LaFe_3O_8$. The electrostatic potentials along the diffusion paths are negative for $Ca_2Fe_2O_5$ and positive for $Sr_2Fe_2O_5$ and $Sr_2LaFe_3O_8$. Therefore, for a negatively charged oxygen species, its diffusion along the channels in $Sr_2Fe_2O_5$ and $Sr_2LaFe_3O_8$ compounds may be favored by the Coulomb energy, but this is not the case for $Ca_2Fe_2O_5$. Electrochemical experiments confirm that, actually, it is not possible to insert oxygen within the networks of $Ca_2Fe_2O_5$ and $Ca_2LaFe_3O_8$.

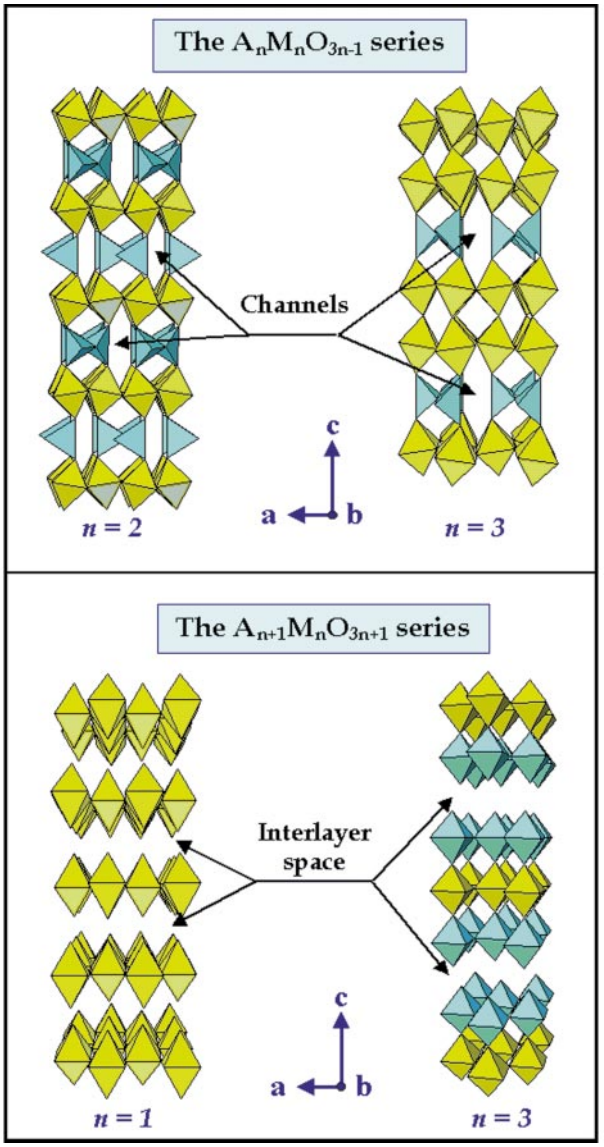

Fig. 5 Representation of the main structural types of the $A_nM_nO_{3n-1}$ and $A_{n+1}M_nO_{3n+1}$ series showing the channels and interlayer space allowing the oxygen intercalation.

Table 1 Some examples of electrochemical oxidation of perovskite-related oxides

Starting material	Electrochemical conditions	Final material	Electrical behavior	Ref.
$A_nM_nO_{3n-1}$-type				
$Sr_2Fe_2O_5$	$E=400$ mV; 60 h	$SrFeO_3$	Metallic	7
Sr_2FeCoO_5	$I=250$ μA; 240 h	Sr_2FeCoO_6	Metallic	8
$Sr_2Co_2O_5$	$E=500$ mV; 180 h	$SrCoO_3$	Metallic	9
$Sr_2LaFe_3O_8$	$E=500$ mV; 190 h	$Sr_2LaFe_3O_{8.95}$	Semi-conducting	10
$YBa_2Cu_3O_{6.50}$	$E=600$ mV; 15 h	$YBa_2Cu_3O_{7-\varepsilon}$	Metallic	11
$A_{n+1}M_nO_{3n+1}$-type				
$La_2CuO_{4.01}$	$E=430$ mV; 120 h	$La_2CuO_{4.09}$	Metal/superconducting	This work
$La_2CuO_{4.01}$	$E=390$ mV; 120 h	$La_2CuO_{4.04}$	Metal/superconducting	This work
$La_2CuO_{4.01}$	$I=10$ μA; 430 h	$La_2CuO_{4.09}$	Metal/superconducting	This work
$La_{2-x}Nd_xCuO_4$	$E=600$ mV; 15 h	$La_{2-x}Nd_xCuO_{4.09}$	Metal/superconducting	12
$La_{2-x}Sr_xCuO_4$	$I=100$ μA cm^{-2}	$La_{2-x}Sr_xCuO_{4+\delta}$	Metal/superconducting	13
$La_{2-x}Ba_xCuO_4$	$I=50$ mA	$La_{2-x}Ba_xCuO_{4+\delta}$	Metal/superconducting	14
Nd_2NiO_4	Potential step (5 mV)	$Nd_2NiO_{4.25}$	Semi-conducting	15
La_2NiO_4	$E=600$ mV; 100 h	$La_2NiO_{4.25}$	Semi-conducting	16
$La_3Ni_2O_7$	$I=10$ μA; 360 h	$La_3Ni_2O_{7.10}$	Metallic	17
$La_4Ni_3O_{10}$	$I=5$ μA; 720 h	$La_4Ni_3O_{10.10}$	Metallic	17

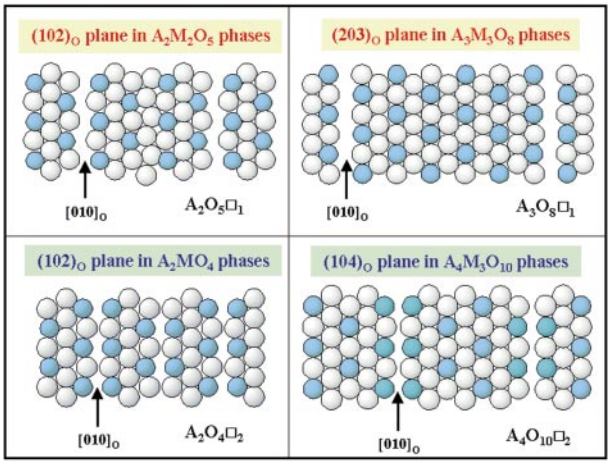

Fig. 6 Representation of the A_xO_y compact hexagonal-type layers showing the missing rows of oxygen constituting the diffusion paths in the perovskite-related compounds.

The Ruddlesden–Popper $A_{n+1}M_nO_{3n+1}$ series. In these compounds, such channels do not appear so clearly, but their structure can be considered as lamellar (Fig. 5), the additional oxygen atoms being inserted into the 'A_2O_2' layers.

From a structural viewpoint, X-ray diffraction analysis shows the materials to remain well crystallized after the electrochemical treatment. This demonstrates the oxygen intercalation to be a topotactic reaction and easy diffusion paths to exist within these structures. Indeed, common features can be found in both series of materials considering that all these structures are based on a stacking of compact hexagonal A_xO_y layers between which metal cations M are located.[18] Then, one can easily notice that oxygen rows along the $[010]_o$ are missing in these layers. Examples are given in Fig. 6. The stacking of these layers finally gives rise to channels in the $A_nM_nO_{3n-1}$ series and rather to interlayer spaces in the $A_{n+1}M_nO_{3n+1}$ series.

Electrochemical oxidation of $A_nM_nO_{3n-1}$ compounds: the example of $Sr_2LaFe_3O_8$

The compounds belonging to the $A_nM_nO_{3n-1}$ series ($n \geqslant 2$) mentioned in Table 1 can be fully oxidized into the corresponding stoichiometric perovskites. All starting materials are almost insulators at room temperature and become semiconductors, metals, or even superconductors upon oxidation.

An interesting example is given by $Sr_2LaFe_3O_8$ ($n=3$ member of the series) which can be oxidized into $Sr_2LaFe_3O_{8.95}$ (cubic perovskite). Mössbauer spectroscopy clearly evidences the drastic changes occurring in the material (Fig. 7). The starting material exhibits, at room temperature, a Mössbauer spectrum characterizing a magnetically ordered compound ($T_N \approx 720$ K) and trivalent iron in octahedral (O_h) and tetrahedral (T_d) sites; the intensity ratio between these lines ($O_h : T_d = 68 : 32$) agrees well with the distribution of iron in both sites with regard to the structure (Fig. 5). Upon electrochemical oxidation, the spectrum undergoes a complete change and no trace of the starting material remains. It exhibits a single peak that can be fitted using a paramagnetic doublet; the Mössbauer parameters reported in Table 2 characterize an averaged valence state (3.63+) evidencing that iron atoms have been oxidized, so that the perovskite compound is formed.

Above a phase transition temperature of 195 K, which can be detected by DSC and magnetic measurements as well as by studying the transport properties (electrical conductivity or Seebeck coefficient; Fig. 8), a fast electron transfer between iron atoms occurs resulting in rather high conductivity.

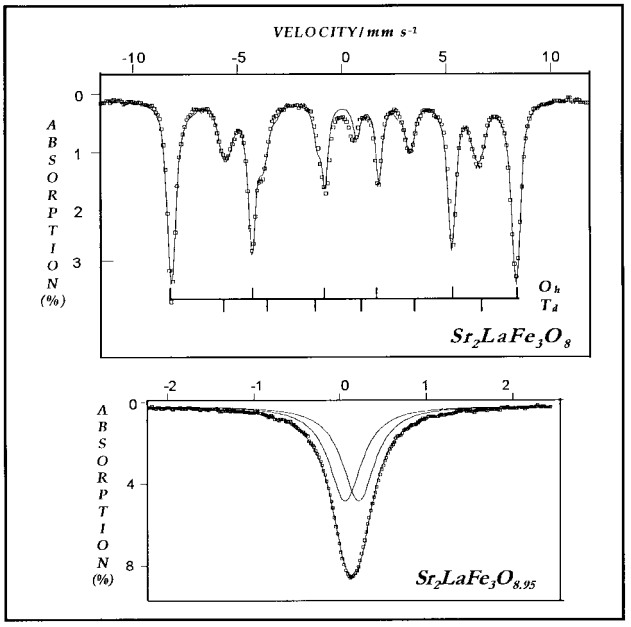

Fig. 7 Mössbauer spectra at 300 K for $Sr_2LaFe_3O_8$ (before electrochemical oxidation) and for $Sr_2LaFe_3O_{8.95}$ (after electrochemical oxidation).

Table 2 Mössbauer parameters of $Sr_2LaFe_3O_{8+\delta}$ phases at room temperature

	Octahedral sites	Tetrahedral sites
$Sr_2LaFe_3O_{8.00}$ (Fe^{3+})	$\delta = 0.35$ mm s^{-1} $H = 51.4$ T	$\delta = 0.18$ mm s^{-1} $H = 37.1$ T
$Sr_2LaFe_3O_{8.95}$ ($Fe^{3.63+}$)	$\delta = 0.14$ mm s^{-1} $\Delta = 0.16$ mm s^{-1}	— —

Electrochemical oxidation of $A_{n+1}M_nO_{3n+1}$ compounds

Unlike the deficient perovskites, the materials belonging to the $A_{n+1}M_nO_{3n+1}$ series are only partly oxidized ($\delta_{max} \approx 0.10$ for cuprates and 0.25 for nickelates) with respect to the number of vacant sites (Table 1), which means that only a few oxygen atoms are inserted in the missing rows (as shown in Fig. 6).

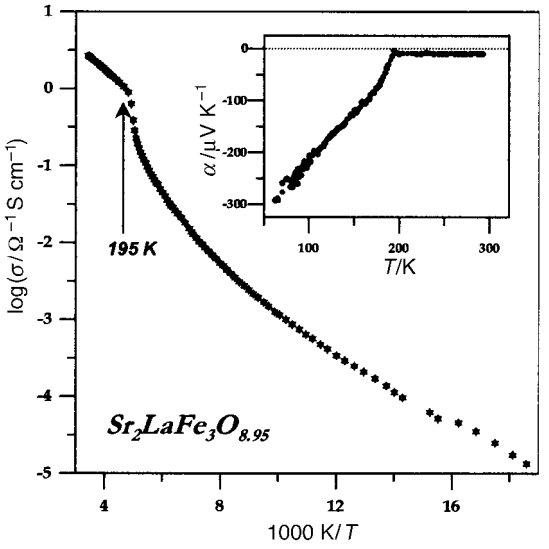

Fig. 8 Temperature dependence of the logarithm of the conductivity for $Sr_2LaFe_3O_{8.95}$. In the inset is represented the temperature dependence of the Seebeck coefficient. The electronic transition is clearly evidenced at 195 K.

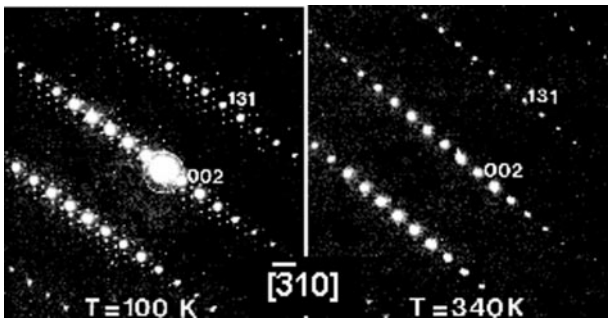

Fig. 9 Electron diffraction patterns for $La_2CuO_{4.09}$, zone axis [$\bar{3}$10]. The low temperature pattern exhibits extra spots which, reversibly, disappear near room temperature.

However, these materials are oxidized to a larger extent than that using high oxygen pressures.

The most interesting feature of these compounds is the oxygen mobility near room temperature. According to the composition δ, it may result in a 'phase separation' which was extensively discussed earlier.[19,20] Thus it appears that given compositions of oxygen excess δ lead to stable phases for which the additional oxygen atoms are ordered. For instance, for the nickelate $La_2NiO_{4+\delta}$, we described in detail the formation of a new phase $La_8Ni_4O_{17}$ ($\delta=0.25$) for which the ordered stage results from an 'electronic' coupling between the oxygen ordering into the La_2O_2 planes and a disproportionation of nickel cations resulting in a charge density wave within the NiO_2 planes.[21] For $La_2CuO_{4+\delta}$ such an ordering was not clearly observed but two line phases were characterized, $\delta=0.04$ and $\delta=0.09$.[22] For the latter, the mobility of oxygen is evidenced using electron microscopy. Fig. 9 shows electron diffraction patterns obtained at 100 K and 340 K: they are obviously different. The low temperature one exhibits extra spots characterizing a commensurate modulated structure which can be interpreted in terms of locally ordered oxygen atoms in the La_2O_2 layers leading to the formation of a giant supercell. At higher temperature, these weak spots disappear, which results from a disordered state of these additional oxygen atoms near room temperature. Upon lowering the temperature these spots reversibly reappear, thus showing the temperature effect on the oxygen mobility.

(b) Electrochemical reduction

La_2MO_4 (M=Ni, Cu) compounds have been widely investigated during the last decade in relation to the superconducting properties exhibited by $La_{2-x}Ba_xCuO_{4+\delta}$.[23] These compounds, annealed in air, show some oxygen overstoichiometry and it finally appears rather difficult to obtain truly stoichiometric samples due to the stabilizing role of these additional oxygen atoms, which has been discussed earlier in terms of structural distortion and electronic effects.[24]

We have previously mentioned the interest in using the electrochemical potential for overoxidizing such materials. Therefore, is it also possible to use such a method for deintercalating these oxygen atoms? Is the electrochemical oxidation a reversible process?

Various compositions of the $La_2Cu_{1-x}Ni_xO_4$ system were at first prepared by solid state reaction of nitrates, then pellets were sintered at 1080 °C for compositions $x<0.25$ and at 1250 °C for $x\geqslant0.25$. Chemical analysis by iodometry of the oxidation state of the cations led to the determination of the excess oxygen δ_{iodo} which depends on the composition (Fig. 10).

Electrochemical experiments were carried out using the galvanostatic mode with a cathodic current of -10 μA. The time dependence of the potential for typical x values is reported in Fig. 11. All of them are similar and exhibit a drastic decrease

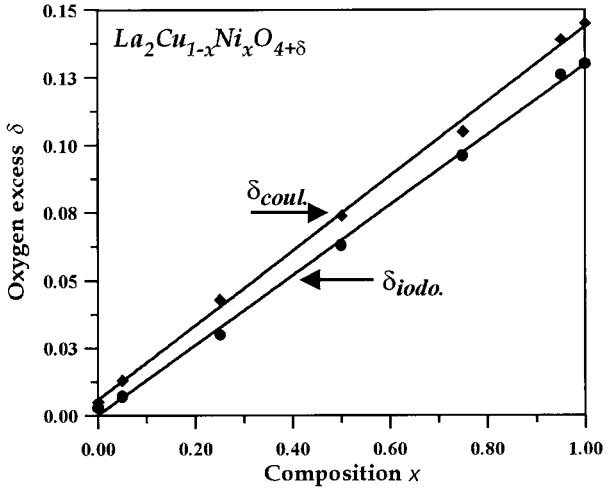

Fig. 10 Composition dependence of the oxygen excess (δ) for the $La_2Cu_{1-x}Ni_xO_{4+\delta}$ system, measured either by iodometry or by coulometry.

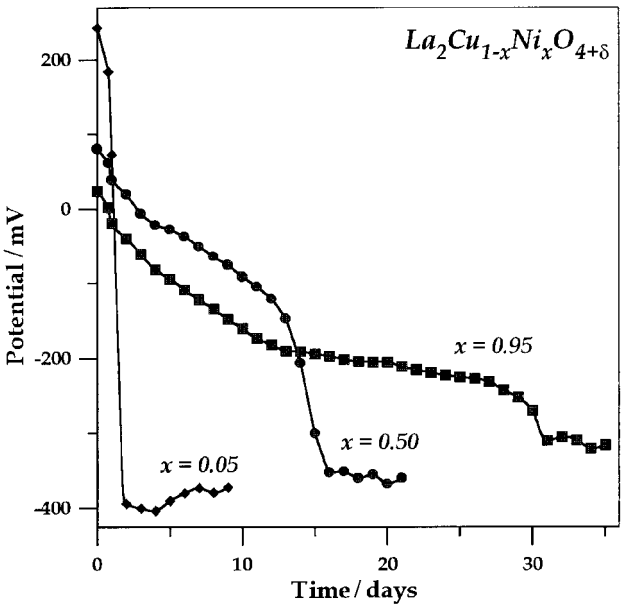

Fig. 11 Time dependences of the potential for typical compositions of the $La_2Cu_{1-x}Ni_xO_{4+\delta}$ system (galvanostatic experiments $I=-10$ μA).

of the potential down to a constant value, which characterizes the end of the reduction of the material. This step occurs after a polarization time which depends on the composition of the starting compound. Then the samples were chemically analyzed; their oxygen stoichiometry was found to be equal to 4.00 within experimental error, which shows that all the excess oxygen was electrochemically removed. The overall reaction can be written as follows:

$$La_2Cu_{1-x}Ni_xO_{4+\delta}+\delta H_2O+2\delta\,e^- \rightarrow La_2Cu_{1-x}Ni_xO_{4.00}+2\delta OH^- \quad (3)$$

In addition, on the basis of this reaction, the value of δ in the starting materials can be calculated from the overall charge transfer ($Q=It_r$), t_r being the polarization time considered when the potential reaches a steady negative value. Thus it follows that:

$$\delta_{coul}=It_rM/2Fm$$

in which I is the current intensity (in this example -10 μA), M is the molar mass of the starting compound, F is the Faraday constant (96484 C) and m is the sample mass. The

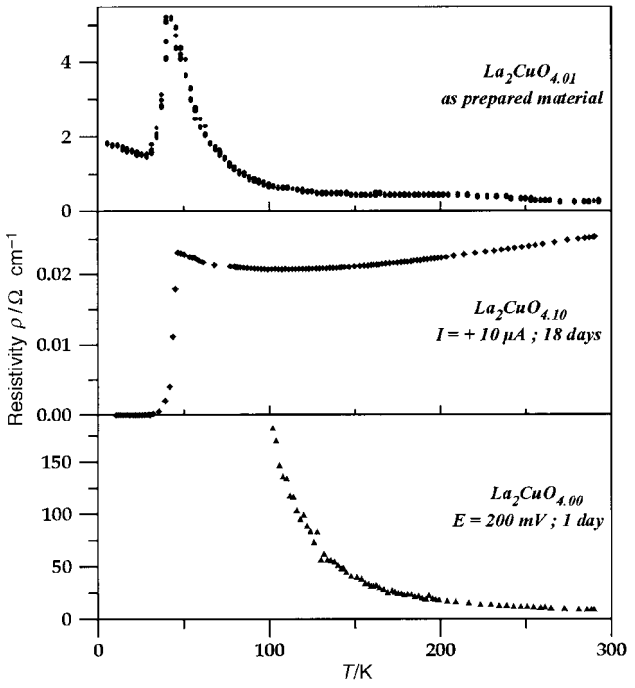

Fig. 12 Thermal dependence of the electrical conductivity for as-prepared, electrochemically oxidized and electrochemically reduced $La_2CuO_{4+\delta}$.

values of δ_{coul} reported in Fig. 10 show a very good agreement with those determined by chemical analysis, which confirms the exchange of 2δ electrons according to electrochemical reaction (3) and that it is really oxygen atoms that are deintercalated.

In addition this is corroborated by following the changes in the properties of the materials such as for instance the electrical conductivity of $La_2CuO_{4+\delta}$ compounds. The as-prepared material $La_2CuO_{4.01}$ exhibits a characteristic semiconducting behavior with a large hump at about 40 K, indicative of filamentary superconductivity (Fig. 12). Galvanostatic oxidation at 10 μA for 18 days leads to a metallic compound $La_2CuO_{4.09}$ which undergoes a superconducting transition at 44 K. Then electrochemical reduction at steady potential, 200 mV, for 1 day, deintercalates all the oxygen atoms as shown by the perfectly semiconducting behavior of the resistivity characterizing the stoichiometric $La_2CuO_{4.00}$ (Fig. 12).

In the same way, the lanthanum nickelate prepared in air shows a large oxygen excess ($\delta \approx 0.14$) and the stoichiometric compound can be obtained by reduction using H_2 or CO/CO_2 (*i.e.* under controlled oxygen pressure) at about 400 °C.[25] Previous works reported this phase to be a 3D antiferromagnetic oxide with $T_N = 328$ K, the magnetic properties depending strongly on the oxygen excess (δ).[25,26] The galvanostatic reduction of $La_2NiO_{4.14}$, $I = -200$ μA for 3 days, leads to a brown sample. XRD analysis confirms the orthorhombic symmetry (*Bmab*) characterizing the stoichiometric oxide $La_2NiO_{4.00}$. The thermal dependence of the magnetic susceptibility shown in Fig. 13 reveals again an important change; the kink observed near 325 K confirms previous determinations of T_N.

Both examples demonstrate the efficiency of this method that can easily control the oxygen stoichiometry of this kind of material as well as the reversibility of the oxygen intercalation.

(c) Oxidation by NO_2 gas

Previous examples were concerned with electrochemically monitored reactions in aqueous solutions. Oxidative deintercal-

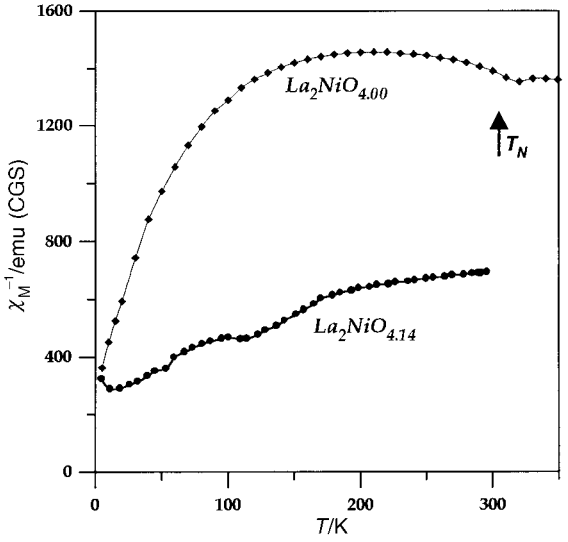

Fig. 13 Thermal dependence of the reciprocal magnetic susceptibility of as-prepared and electrochemically reduced $La_2NiO_{4+\delta}$.

ation processes can also be achieved using chemical agents: the most well known example is the lithium deintercalation from some oxide (*e.g.* $LiCoO_2$ or $LiNbO_2$) or sulfide (*e.g.* $LiTiS_2$) networks using strong oxidizing agents such as I_2, Br_2, MoF_6, etc. in acetonitrile.[27–29] One can also mention oxidizing intercalation processes in aqueous solutions containing species such as MnO_4^-, BrO^- or ClO^- which were used, for instance, for overoxidizing cuprates such as $La_2CuO_{4+\delta}$ or $LaCuO_{2+\delta}$.[30,31]

However, another way is a solid–gas reaction at moderate temperatures ($T \leqslant 350$ °C). In this temperature range, the kinetics with O_2 is generally slow and one can use F_2 or Cl_2 instead but decomposition of the materials is often observed. We recently investigated an alternative reaction involving gaseous NO_2 and more especially its reaction with ammonium ions NH_4^+.[32] Actually such a process implies the N^{+IV}/N^{-III} redox couple as in the explosive decomposition of NH_4NO_3; in addition we may expect the *in situ* destruction of NH_4^+ in the starting materials according to the following reaction:

$$NO_{2(g)} + NH_4^+ + e^- \rightarrow N_2\uparrow + 2H_2O\uparrow \quad (4)$$

This mole-to-mole reaction yields neutral species, *i.e.* gaseous H_2O and N_2, as by-products that can be easily expelled from the material with respect to their size which is close to that of NH_4^+ cations. Therefore one can presume a topotactic destruction of these large cations leaving large empty sites in the final compound. One should also note that this redox reaction requires one electron.

Typically, powders of the starting material deposited on a sintered glass are treated at temperatures ranging between 20 and 350 °C by a mixture of NO_2–N_2. Depending on the materials, the reaction can be violent. Various kinds of reactions have been carried out; they can be classified as follows.

Topotactic reactions

The initial structure remains unchanged after the *in situ* destruction of NH_4^+. The first example concerns the hexagonal tungsten bronzes $(NH_4)_xWO_3$ that are prepared by controlled reduction of $(NH_4)_{10}W_{12}O_{41}\cdot 5H_2O$ under Ar–H_2 (10%) at *ca.* 380 °C. The composition x determined by TGA and the Kjeldahl method is close to 0.20. Then a treatment of this dark blue sample with NO_2, for 3 h, near 250–300 °C leads to a well crystallized white powder, this color being characteristic of the oxidation of the cations from W^{5+} to W^{6+}. The absence of ammonium ions was checked by the Kjeldahl method and various physical characterizations (IR, mass spectrometry)

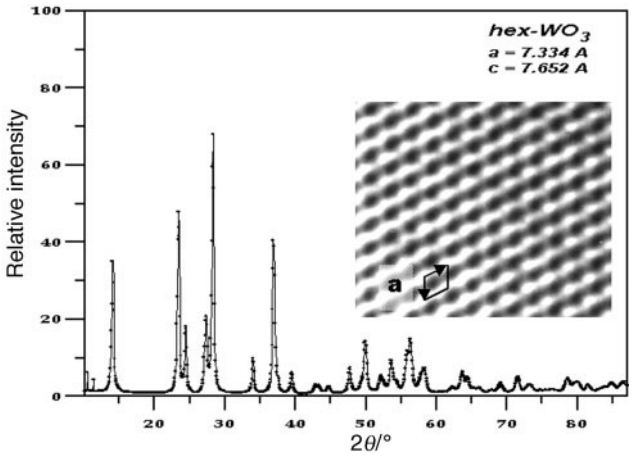

Fig. 14 X-Ray diffractogram of hexagonal WO_3. The inset shows a high resolution electron diffraction image ([001] zone axis).

reveal that the final compound is a hexagonal form of WO_3. This is confirmed by the X-ray diffraction pattern as well as by the electron microscopy image (Fig. 14) showing the large tunnels of the structure (Fig. 15). The lattice parameters (a = 7.334 Å, c = 7.652 Å) are somewhat different from those previously reported for h-WO_3 obtained by a reconstructive process (dehydration of $WO_3 \cdot 1/3H_2O$, a = 7.298 Å, c = 7.798 Å), the c parameter being unambiguously doubled.[33]

The second example deals with ammonium molybdenum oxide; the starting compound is obtained from $Na_2MoO_4 \cdot 2H_2O$ by cationic exchange in a solution of NH_4Cl, the resulting material being ammonium and molybdenum deficient with a composition close to $(NH_4)_{0.7}Mo_{5.3}O_{18}H_{3.4}$, but containing only Mo^{+VI}.[34] XRD analysis shows a single phase with hexagonal symmetry (a = 10.583 Å, c = 3.724 Å). The NO_2 treatment (3 h, 150 to 300 °C) again retains the parent structure and the final material was identified to be pure hexagonal MoO_3 (Fig. 15). One should point out that in this case no oxidation of the cation is required, which raises the question of the provenance of the electron in reaction (4). There could be two explanations: either there is an oxidation of oxygen anions according to $O^{2-} \rightarrow \frac{1}{2}O_2 + 2e^-$, reaction (4) remaining the basic one, or the reaction with NO_2 occurs *via* a two step process, the first being the destruction of NH_3 leading to the formation of a hydrate or hydroxide without oxidation of the material, according to a scheme which only involves an internal redox process:

$$4NH_4^+ + 3NO_{2(g)} \rightarrow 4H^+ + 7/2N_2\uparrow + 6H_2O\uparrow \qquad (5)$$

Then this hydrate or hydroxide can be thermally decomposed at moderate temperatures.

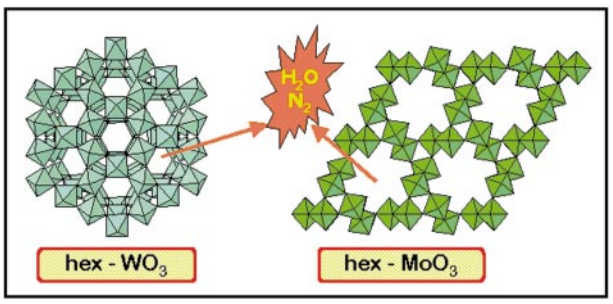

Fig. 15 Hexagonal structures of WO_3 and MoO_3 showing the large empty channels after NO_2 treatment.

Non-topotactic reactions

As pointed out, the reaction of ammonium compounds may sometimes be violent, resulting in destruction of the parent structure. Two examples can be quoted.

NH_4VO_3 crystallizes with the structure of α-$NaVO_3$ made of (VO_4) chains of tetrahedra; this compound was treated by NO_2 at various temperatures. At 100 °C, within a few minutes, it is transformed into the well crystallized α-V_2O_5 whose lamellar structure is completely different from that of the starting material (V^{5+} cations are located in corner-sharing pyramids).[35]

In the same way, starting from ammonium cerium nitrate $(NH_4)_2Ce(NO_3)_6$, one can prepare cerium oxide CeO_2, at typically 200–300 °C, by NO_2 treatment for about 1 hour. The X-ray diffraction pattern reveals a poorly crystallized material (Fig. 16). SEM images show a particle size of about 0.1–0.2 μm. With respect to its industrial applications (catalysis, ionic conductor in solid oxide fuel cells), the preparation of this oxide with such a submicronic texture is of great interest.[36]

Obviously the use of NO_2 gas as oxidizing agent at moderate temperatures and more especially its exothermic reaction with ammonium compounds opens a large field of investigation for preparing oxides in metastable forms or with peculiar textures.

(d) Chemical reduction by borohydride solution

The synthesis of oxides containing metal cations with low oxidation states usually requires solid state reactions at high temperatures under reducing atmosphere (*i.e.* low oxygen partial pressure p_{O_2}) generated by CO/CO_2 or H_2, NH_3, *etc.* For preparing metastable phases, at about room temperature, alternative routes should be used. We mentioned above the electrochemical reduction that allows the deintercalation of oxygen but also the intercalation of cations such as H^+ or Li^+ in materials devoted to applications in electrochromism or batteries. Often, the latter reaction is achieved in non-aqueous solvents; however chemical reduction of oxides has also been considered in aqueous solutions. Various reducing agents can be used; one can quote, for instance, Zn or sulfites which have been recognized for their efficiency, especially for preparing metals.[37] Recently borohydride solutions have been

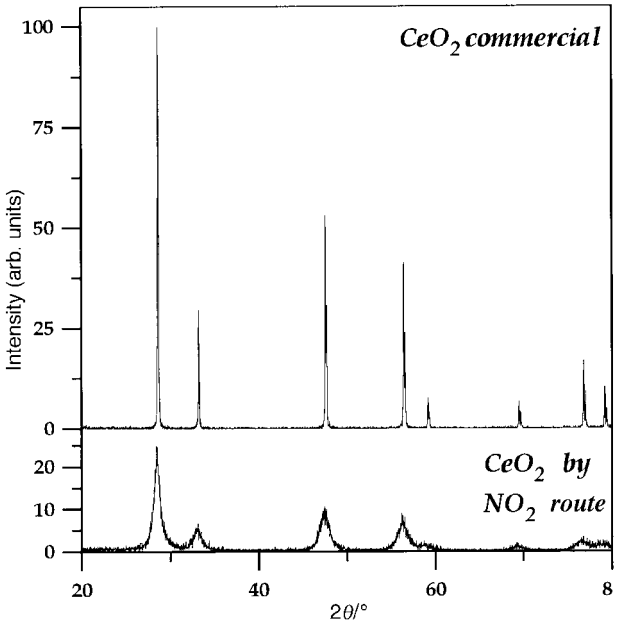

Fig. 16 X-Ray diffractograms of the commercial cerium oxide and that obtained by the NO_2 route.

reassessed for the preparation of nanoparticles and low valent oxides at room temperature.[38–40]

According to the thermodynamical data, the redox potential of the following reaction:

$$H_2BO_3^- + 5H_2O + 8e^- \Leftrightarrow BH_4^- + 8OH^-$$

is $E_0 = -1.24$ V *vs.* SHE.[37] With regard to this high value and in order to prevent water decomposition, sodium or potassium borohydrides should be stabilized in alkaline solution.

Various kinds of reactions can be achieved; recently, Zhang and Manthiram[38] reported the preparation of M–boron nanoparticles (M = Fe, Co, Ni) and we also obtained amorphous cobalt by this method. With respect to the reduction of oxides, the nature of the reaction products as well as the texture of the materials seem to depend drastically on the concentration of the solutions and on the pH. Often the synthesized oxides are amorphous, which, for applications such as in batteries, is advantageous. Thus Tsang and Manthiram prepared MoO_2 and VO_2(B) whose cyclability makes these compounds attractive for Li batteries.[40,41]

Another interesting application of these borohydride reducing solutions is the preparation of crystallized oxides at room temperature, which we recently developed.[42] Two kinds of experiments have been carried out: in the first, the starting oxide is dissolved beforehand, whereas in the second it is not.

(1) Preparation of $(NH_4)_2V_3O_8$ by precipitation

The starting material α-V_2O_5 is dissolved at first in 1 M KOH solution. NH_4Cl is then added in excess, the pH being close to 10.5. The reduction of V^{5+} to V^{4+} is obtained by addition of the solution of $NaBH_4$ under nitrogen atmosphere. At last, the pH is slowly lowered down to 7.5 by adding dilute HCl and black ammonium vanadyl vanadate $(NH_4)_2V_3O_8$ precipitates. After filtration, washing and drying, the material is characterized by chemical analysis and TGA and its X-ray diffraction pattern shows a rather well crystallized compound (Fig. 17). It is identified as the 'black hydrate of vanadium' synthesized earlier by reduction, at 100 °C, for 24 hours, using Zn as reducing agent.[43] One should point out that our method leads within 1 hour to a similar result.

The structure of this compound is built up of 'V_3O_8' sheets formed from the condensation and reduction of $(VO_4)^{3-}$ soluble species, between which ammonium ions are inserted as pillars. It is quite different from that of α-V_2O_5.

One should point out that, in more or less similar conditions, Zhu and Manthiram prepared Na_xWO_3, which was amorphous,[44] which emphasizes that experimental conditions are of vital importance.

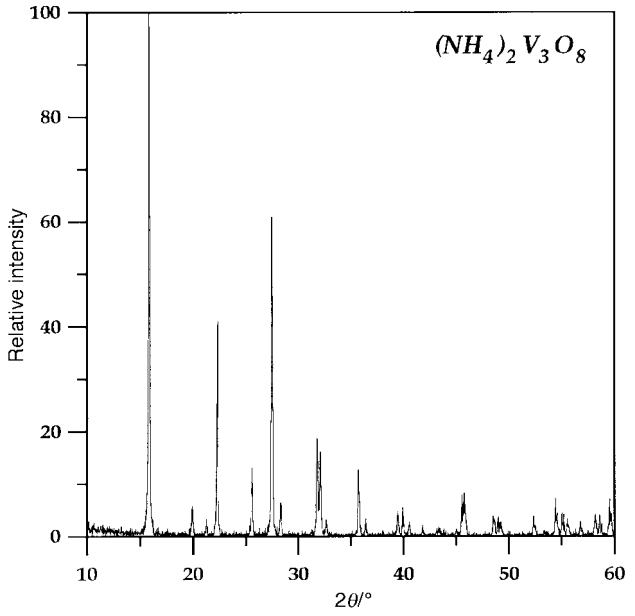

Fig. 17 X-Ray diffractogram of $(NH_4)_2V_3O_8$ prepared by the borohydride method.

(2) Preparation of K_xWO_3: a topotactic reduction

We described above the preparation of hexagonal WO_3: this compound contains large tunnels in which various chemical species can be easily inserted.[45] The reduction by KBH_4 is carried out in a solution in which h-WO_3 has been mixed with an excess of KCl. The pH is kept close to 7.5. Within a few minutes the white starting material becomes blue. The powder is then filtered and dried. X-Ray diffraction confirms that the hexagonal structure is preserved. Electron microprobe analysis leads to a potassium content close to 0.27 in agreement with the value expected from the addition of borohydride ($x \approx 0.30$).

This example clearly demonstrates that borohydride solutions can provide an interesting route for intercalating cations such as Li^+, Na^+, K^+ or NH_4^+ into oxide networks using aqueous solutions instead of other routes such as butyllithium in organic solvents.

Conclusion

The development of '*chimie douce*' preparative methods in solid state chemistry has undoubtedly broadened the field of new materials either in a metastable form or with particular textures, which cannot be obtained by other routes. This is due to the fact that the nature of the reaction products is controlled by kinetics rather than by thermodynamics. These methods can be classified into two main types: those using the electrochemical potential as the driving force and those based on chemical redox reactions.

For transition metal oxides, provided that the crystal structure accommodates diffusion paths for oxygen ions, it is possible to tune the oxygen stoichiometry over a large range and hence to promote interesting properties such as superconductivity.

NO_2 gas as well as borohydrides are basic reactants in chemistry, but, surprisingly, they have not been much used in solid state chemistry. We described some attractive reactions, which may open new fields of investigations at moderate temperatures. The solid–gas reaction of NO_2 with ammonium compounds leads to two types of processes: those for which the *in situ* destruction of NH_4^+ is topotactic and those where the precursor structures collapse giving rise to more stable compounds or to amorphous or finely divided materials.

Finally, the use of borohydride aqueous solutions for reducing oxides appears simple and efficient; it generally yields nanotextured materials interesting for various applications such as catalysis or energy storage in batteries.

The authors thank the Rhône-Poulenc company for financial support and are very grateful to C. Monroux, Y. Muraoka, P. Dordor, A. Demourgues, F. Arrouy, E. Marquestaut, M. D. Carvolho and F. M. A. Costa for their helpful contributions to this work.

References

1 *Soft chemistry routes to new materials*, *Mater. Sci. Forum*, 1994, **152–153**, ed. J. Rouxel, M. Tournoux and R. Brec, Trans Tech Publications, USA.
2 J-C. Grenier, A. Wattiaux, J-P. Doumerc, P. Dordor, L. Fournès, J-P. Chaminade and M. Pouchard, *J. Solid State Chem.*, 1992, **96**, 20.
3 M. Izaki and T. Omi, *J. Electrochem. Soc.*, 1997, **144**, 1949.
4 A. Wattiaux, J-C. Park, J-C. Grenier and M. Pouchard, *C. R. Acad. Sci. Paris*, 1990, **310**, 1047.

5 J. O'M. Bockris and T. Otagawa, *J. Electrochem. Soc.*, 1984, **131**, 290.
6 M. Armand, *Intercalation in Materials for Advanced Batteries*, ed. D. W. Murphy, Plenum New York, 1980, p. 145.
7 A. Wattiaux, L. Fournes, A. Demourgues, N. Bernaben, J-C. Grenier and M. Pouchard, *Solid State Commun.*, 1991, **77**, 489.
8 P. Bezdicka, L. Fournes, A. Wattiaux, J. C. Grenier and M. Pouchard, *Solid State Commun.*, 1994, **91**, 501.
9 P. Bezdicka, A. Wattiaux, J. C. Grenier, M. Pouchard and P. Hagenmuller, *Z. Anorg. Allg. Chem.*, 1993, **619**, 7.
10 A. Wattiaux, L. Fournès, F. Zhou, J-C. Grenier, M. Pouchard and J. Etourneau, *J. Phys. IV Fr.*, 1997, **7**, C1351.
11 J. C. Park, A. Wattiaux, J. C. Grenier, K. Fröhlich, P. Dordor, M. Pouchard and P. Hagenmuller, *Z. Anorg. Allg. Chem.*, 1992, **608**, 153.
12 F. Arrouy, A. Wattiaux, E. Marquestaut, C. Cros, G. Demazeau, J-C. Grenier and M. Pouchard, *J. Solid State Chem.*, 1995, **115**, 140.
13 F. C. Chou, J. H. Cho and D. C. Johnston, *Physica C*, 1992, **197**, 303.
14 M. Itoh, Y. J. Shan, S. Sakamoto, Y. Inaguma and T. Nakamura, *Physica C*, 1994, **223**, 75.
15 S. Bhavaraju, J. D. DiCarlo, D. P. Scarfe, I. Yazdi and A. J. Jacobson, *Chem. Mater.*, 1994, **6**, 2172.
16 A. Demourgues, A. Wattiaux, J-C. Grenier, M. Pouchard, J-M. Dance and P. Hagenmuller, *J. Solid State Chem.*, 1993, **105**, 458.
17 M. D. Carvalho, F. M. A. Costa, I. S. Pereira, A. Wattiaux, J. M. Bassat, J-C. Grenier and M. Pouchard, to be published.
18 C. Dussaret, F. Grasset and J. Darriet, *Eur. J. Solid State Inorg. Chem.*, 1995, **32**, 557.
19 *Phase separation in cuprate superconductors*, ed. K. A. Müller and G. Benedeck, World Scientific, Singapore, 1992.
20 *Phase separation in cuprate superconductors*, ed. E. Sigmund and K. A. Müller, Springer Verlag, Berlin, 1994.
21 A. Demourgues, F. Weill, B. Darriet, A. Wattiaux, J-C. Grenier, P. Gravereau and M. Pouchard, *J. Solid State Chem.*, 1993, **105**, 317, 330.
22 C. Monroux, A. Wattiaux and J-C. Grenier, to be published.
23 J. G. Bednorz and K. A. Müller, *Z. Phys. B*, 1986, **64**, 189.
24 J. C. Grenier, F. Arrouy, J-P. Locquet, C. Monroux, M. Pouchard, A. Villesuzanne and A. Wattiaux, *Phase separation in cuprate superconductors*, ed. K. A. Müller Benedeck, World Scientific, Singapore, 1994, p. 237.
25 S. Hosoya, T. Omata, K. Nakajima, K. Yamada and Y. Endoh, *Physica C*, 1992, **202**, 188.
26 A. Demourgues, P. Dordor, J-P. Doumerc, J-C. Grenier, E. Marquestaut, M. Pouchard, A. Villesuzanne and A. Wattiaux, *J. Solid State Chem.*, 1996, **124**, 199.
27 G. G. Amatucci, J. M. Tarascon and L. C. Klein, *J. Electrochem. Soc.*, 1996, **143**, 1114.
28 R. Gupta and A. Manthiram, *J. Solid State Chem.*, 1996, **121**, 483.
29 A. R. Wizansky, P. E. Rauch and F. J. Disalvo, *J. Solid State Chem.*, 1989, **81**, 203.
30 E. Takayama-Muromachi, T. Sasaki and Y. Matsui, *Physica C*, 1993, **207**, 97.
31 M. Trari, J. Töpfer, J-P. Doumerc, M. Pouchard, A. Ammar and P. Hagenmuller, *J. Solid State Chem.*, 1994, **111**, 104.
32 S. Petit, J-P. Doumerc, J-C. Grenier, T. Séguelong and M. Pouchard, *C.R. Acad. Sci. Paris*, *Ser. IIb*, 1995, **321**, 37.
33 B. Gérand, G. Novogrocki, J. Guenot and M. Figlarz, *J. Solid State Chem.*, 1979, **29**, 429.
34 Y. Muraoka, J-C. Grenier, S. Petit and M. Pouchard, *Eur. J. Solid State Inorg. Chem.*, submitted.
35 S. Petit, J. P. Doumerc, J. C. Grenier and M. Pouchard, *C. R. Acad. Sci.*, in press.
36 J-P. Doumerc, J-C. Grenier, M. Pouchard and S. Petit, Rhône-Poulenc Chimie, *Fr. Pat.*, 95-01874, 1995.
37 *Handbook of Chemistry and Physics*, ed. R. C. Weast, CRC Press, Cleveland, OH, 56th edn., 1976, D146.
38 L. Zhang and A. Manthiram, *J. Mater. Chem.*, 1996, **6**, 999.
39 C. Tsang, A. Dananjay, J. Kim and A. Manthiram, *Inorg. Chem.*, 1996, **35**, 504.
40 A. Manthiram and Y. T. Zhu, *J. Electrochem. Soc.*, 1996, **143**, L143.
41 C. Tsang and A. Manthiram, *J. Electrochem. Soc.*, 1997, **144**, 520.
42 S. Petit, K. David, J-P. Doumerc, J-C. Grenier, T. Séguelong and M. Pouchard, *C.R. Acad. Sci. Paris*, *Ser. IIc*, 1998, **1**, 517.
43 J. Bernard and F. Théobald, *C. R. Acad. Sci. Paris*, 1963, 4916.
44 Y. T. Zhu and A. Manthiram, *J. Solid State Chem.*, 1994, **110**, 187.
45 S. Petit, B. Jousseaume, L. Fournès, J. P. Doumerc, J. C. Grenier, A. Wattiaux, M. Pouchard and P. Hagenmuller, *Essays on Interdisciplinary Topics in Natural Sciences*, ed. R. B. Scorzelli, I. Souza Azevedo and E. Baggio Saitovitch, CBPF, Rio de Janeiro, Brazil, 1997, p. 199.

Paper 8/05213A